crystals (*23*), possibly because we are dealing with a singular extended system with large channels, where the factors mentioned above are likely to exert a greater influence on spin conversion than in related molecular systems.

Catenanes are of great interest in topological stereochemistry (*24*), not only for aesthetic or intellectual pleasure but also because of their potential derived properties. Supramolecular systems have attracted the attention of many research groups because of their photochemical (*25*) and magnetic properties that can result from the interaction among their subunits. Detailed structural and magnetic characterization sheds light on the mechanisms leading to these properties, such as the cooperative mechanisms of spin crossover studied here.

REFERENCES AND NOTES

1. E. A. Boudreaux and L. N. Mulay, Eds., *Theory and Applications of Molecular Paramagnetism* (Wiley, New York, 1976).
2. O. Kahn, *Molecular Magnetism* (VCH, New York, 1993).
3. P. Gütlich, *Struct. Bonding (Berlin)* **44**, 83 (1981); P. Gütlich, A. Hauser, H. Spiering, *Angew. Chem. Int. Ed. Engl.* **33**, 2024 (1994).
4. E. König, *Struct. Bonding (Berlin)* **76**, 51 (1991).
5. P. Gütlich and A. Hauser, *Coord. Chem. Rev.* **97**, 1 (1990).
6. E. König, *Prog. Inorg. Chem.* **35**, 527 (1987).
7. F. L. Carter, Ed., *Molecular Electronic Devices* (Dekker, New York, 1982); *Molecular Electronic Devices II* (Dekker, New York, 1987).
8. R. C. Haddon and A. A. Lamola, *Proc. Natl. Acad. Sci. U.S.A.* **82**, 1874 (1985).
9. J. S. Miller, *Adv. Mater.* **2**, 378 (1990); *ibid.*, p. 495; *ibid.*, p. 601.
10. J. Zarembowitch and O. Kahn, *New J. Chem.* **15**, 181 (1991).
11. S. Decurtins, P. Gütlich, C. P. Köhler, H. Spiering, A. Hauser, *Chem. Phys. Lett.* **105**, 1 (1984).
12. J. Zarembowitch *et al.*, *Mol. Cryst. Liq. Cryst.* **234**, 247 (1993).
13. C. Roux, J. Zarembowitch, B. Gallois, T. Granier, R. Claude, *Inorg. Chem.* **33**, 2273 (1994).
14. O. Kahn, J. Kröber, C. Jay, *Adv. Mater.* **4**, 718 (1992).
15. B. Gallois, J. A. Real, C. Hauw, J. Zarembowitch, *Inorg. Chem.* **20**, 1152 (1990).
16. J. A. Real, B. Gallois, T. Granier, F. Suez-Panamá, J. Zarembowitch, *ibid.* **31**, 4972 (1992).
17. T. Granier, B. Gallois, J. Gaultier, J. A. Real, J. Zarembowitch, *ibid.* **32**, 5305 (1993).
18. J. A. Real *et al.*, *J. Am. Chem. Soc.* **114**, 1979 (1992).
19. W. Vreugdenhil *et al.*, *Polyhedron* **9**, 2971 (1990).
20. At present, only a few examples of interpenetrating 2D networks are known. Some of them are shown in the following: J. Konnert and D. Britton, *Inorg. Chem.* **7**, 1193 (1966); R. W. Gable, B. F. Hoskins, R. Robson, *Chem. Commun.* **1990**, 1677 (1990); H. O. Stumpf, L. Ouahab, Y. Pei, D. Grandjean, O. Kahn, *Science* **261**, 447 (1993).
21. The compound $[Fe(tvp)_2(NCS)_2] \cdot CH_3OH$ was synthesized by slow addition of a methanolic solution (30 ml) containing an excess of tvp (6×10^{-3} mol) to a filtered methanolic solution (25 ml) prepared by mixing $Fe(ClO_4)_2 \cdot 6\,H_2O$ (10^{-3} mol) and KNCS (2×10^{-3} mol). The reaction was carried out under continuous stirring at 45°C. A deep red polycrystalline powder appeared in a few minutes. All operations were carried out under an argon atmosphere. The solid, stable in air, was washed with methanol and dried under vacuum.
22. The compound $[Fe(tvp)_2(NCS)_2] \cdot CH_3OH$ crystallizes in the tetragonal system, space group *P4/ncc* (number 130), with $a = b = 15.977(5)$ Å and $c = 15.368(4)$ Å (the number in parentheses is the error in the last digit), $V = 3922.9$ Å^3, $Z = 4$, $d_{calc} = 0.908$ g cm^{-3}, and λ (Mo Kα) = 0.71073 Å. The structure was solved by direct methods and successive Fourier difference syntheses. The refinements by full-matrix least-squares gave an *R* factor of 8.3 and a weighted *R* factor (R_w) of 6.5 from 860 reflections with intensity $I \geq 3\sigma(I)$ for 129 variables [weight = $9.5758/\sigma^2(F)$]; linear absorption coefficient μ (Mo Kα) = 8.64 cm^{-1}. All nonhydrogen atoms were refined anisotropically. The methanol molecules are disordered; our recent x-ray single-crystal analysis on isostructural $[Co(tvp)_2(NCS)_2] \cdot CH_3OH$ confirms the number of solvent molecules per complex.
23. Sample A is obtained as a polycrystalline powder [see (*21*)]. Sample B consists of large single crystals obtained from slow diffusion (3 to 4 weeks) as mentioned above. Analytical data and x-ray powder diffraction of the different samples are the same, although significant differences can be observed in their magnetic curves.
24. G. Schill, *Catenanes, Rotaxanes, and Knots* (Academic Press, New York, 1971); D. M. Walba, *Tetrahedron* **41**, 3166 (1985); J. P. Sauvage, *Acc. Chem. Res.* **23**, 319 (1990); J. P. Sauvage *et al.*, *Chem. Rev.* **94**, 993 (1994).
25. V. Balzani and F. Scandola, *Supramolecular Photochemistry* (Horwood, Chichester, 1991).
26. We acknowledge financial assistance from the Dirección General de Investigación Científica y Técnica (DGICYT) (Spain) through Project PB91-0807-C02-01 and the Human Capital and Mobility Program (Network on Magnetic Molecular Materials from the EEC) through grant ERBCHRXCT920080. We are deeply indebted to J. Zarembowitch for her help in reviewing this contribution.

11 November 1994; accepted 10 February 1995

Imaging the Condensation and Evaporation of Molecularly Thin Films of Water with Nanometer Resolution

J. Hu,* X.-D. Xiao, D. F. Ogletree, M. Salmeron

The polarization force between an electrically charged atomic force microscope tip and a substrate has been used to follow the processes of condensation and evaporation of a monolayer of water on mica at room temperature. Condensation proceeds in two distinct structural phases. Up to about 25 percent humidity, the water film grows by forming two-dimensional clusters of less than a few 1000 angstroms in diameter. Above about 25 percent humidity, a second phase grows, forming large two-dimensional islands with geometrical shapes in epitaxial relation with the underlaying mica lattice. The growth of this second water phase is completed when the humidity reaches about 45 percent. The reverse process of evaporation has also been imaged.

The nanometer-scale structure of liquid films and surfaces is a fundamental subject of materials and biological sciences that has until now eluded a direct study because of the lack of suitable microscopy techniques with the required level of resolution. The growth of thin films of water is an important and largely unsolved problem in physics, chemistry, and biology. Water films alter the adhesion and lubricating properties of surfaces and the reactivity of solids with ambient gas molecules. The contact angle of water is used as a measure of the chemical activity of the surface. In biological processes, water films are critical for ion transport. Several studies have been recently devoted to the layering and orientation of water molecules on surfaces (*1–4*). Ice-like structures are predicted for the first layers, but no experimental evidence is available (*5–9*). Imaging water surfaces with nanometer resolution would make it possible to study many basic aspects of wetting, including condensation, evaporation, and chemical reactions. The validity of growth models and the structure of the first layers could be investigated at the molecular level.

Although modern scanning probe microscopes, like the scanning tunneling microscope (STM) and the atomic force microscope (AFM), have atomic-scale resolution, they cannot be easily used to study free liquid surfaces. For liquids, if the probe tip comes into contact with the surface, strong capillarity forces will cause the liquid to wet the tip and will strongly perturb the liquid. To avoid the bulging of the liquid surface that leads to wetting and capillary interaction, the tip must be kept at least several tens of angstroms from the imaging surface.

Our approach has been to use electrical polarization forces by applying a voltage to a conductive AFM tip with respect to a remote grounded electrode, for example, the sample holder (*10*). The strong electric field around the charged tip induces a polarization charge distribution on the surface of any nearby conductive or insulating materials. Because of the long-range nature of electrostatic interactions, the force can be detected at distances of several hundred of angstroms from the surface. This distance was determined by measuring the displacement of the

---

Materials Sciences Division, Lawrence Berkeley Laboratory, Berkeley, CA 94720, USA.

*Permanent address: Shanghai Institute of Nuclear Research, Academia Sinica, Post Office Box 800-204, Shanghai 201800, China.

sample that brings tip and surface into contact when both are electrically neutral. Topographic images can be obtained by maintaining the polarization force constant through feedback control of the tip-sample distance [we used a commercial RHK (Rochester Hills, Michigan) STM-100 unit]. We obtained a vertical resolution of ~0.5 Å. With this imaging technique, we have been able to image the structures formed by the condensation and evaporation of water on mica surfaces. Because polarizability is a material property, when layers of one material are imaged on a substrate of a different material, its apparent height or image contrast is modified by the dielectric constant of the materials being imaged. If the overlayer being imaged has a dielectric constant that is greater than that of the substrate, its apparent height will be greater than its topographic height. Conversely, if the dielectric constant of the material on the surface is smaller, its apparent height will be reduced. For molecularly thin layers, the ratio between real and apparent heights can differ by a factor of order 10 (*11*).

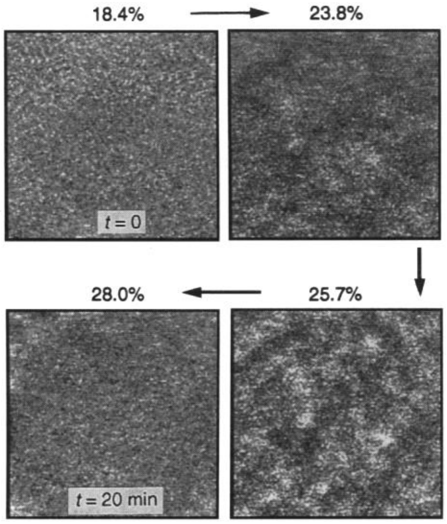

Fig. 1. A series of 2.5 μm by 2.5 μm images of mica exposed to water vapor at room temperature (21°C), obtained by an AFM with a charged tip (−2.5 V) operating at a distance of ~200 Å. At time *t* = 0, the mica is cleaved at 18.4% relative humidity. No contrast was observed above the noise level (0.5 Å). At higher humidities, 2D clusters formed with diameters of up to 1000 Å and apparent heights of ~2 Å. The number of these clusters increased with humidity until they completely covered the surface. In this experiment, this effect is seen at 28% humidity. We refer to this as phase I water.

The water-imaging experiments were carried out at room temperature (21°C) in an environmental chamber housing the AFM. Low humidity was achieved by introducing a desiccant material and by flowing dry nitrogen. High humidity was achieved by evaporating water from a beaker. We used commercial Si_3N_4 cantilevers with a nominal force constant of ~0.58 N/m, coated with a 100 Å Pt film for electrical conductivity. The mica samples were prepared by cleavage and were typically several tenths of a millimeter thick. Mica is an anisotropic material with an average dielectric constant of 7. The images were taken at a tip voltage of ±2 to ±3V, which results in an attractive force of ~10 nN at a tip-surface distance of ~200 Å. The lateral resolution is of the same order. No dependence of the image on the sign of the applied bias was found for electrically neutral surfaces. When the AFM was operated in the usual contact mode in identical humidity conditions, only the mica lattice could be seen. This indicates the strong perturbation of the water film by the tip upon contact. In our imaging conditions, no perturbation of the structure of the water film was observed.

Immediately after cleavage at 18% humidity, the surface showed no contrast above the noise level (0.5 Å) (Fig. 1). As the humidity increased monotonically, many two-dimensional (2D) clusters formed with apparent heights of ~2 Å. The diameter of the clusters varied from 100 Å (our resolution limit) up to a few thousand angstroms. The number of clusters grew gradually until there was a uniform layer when the humidity reached 28%. At this stage, the image contrast disappeared. We call this structure phase I. In other experiments, phase I completed its formation at humidities ranging from 22 to 28%. In some cases, the formation of clusters was not observed and the images remained featureless until the saturation of phase I. This variability is probably due to adsorption of impurities and to local temperature fluctuations caused by the laser beam impinging on the cantilever.

As the humidity continued to increase,

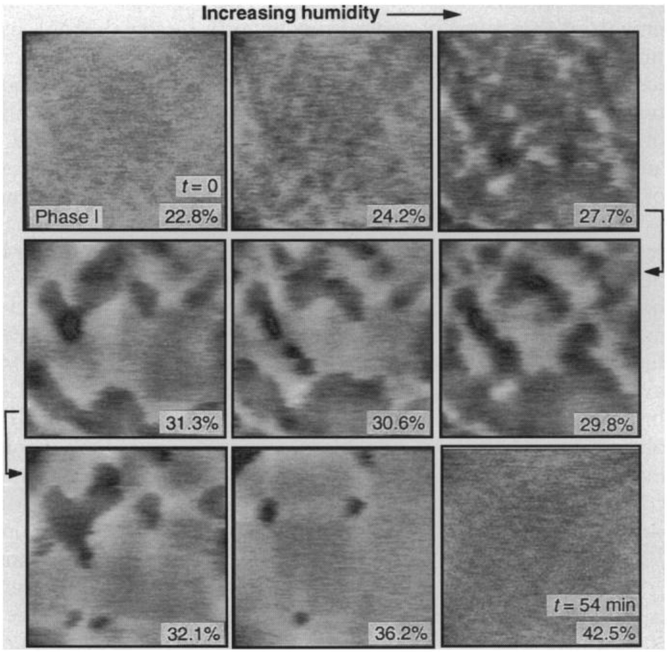

Fig. 2. Growth of water on mica at humidities above 23% in a series of 2.5 μm by 2.5 μm images. At *t* = 0, a phase I layer has been completed. As humidity increases (value at bottom right of each image), phase II grows in 2D domains (bright regions) that increase in size and number. The apparent height of these domains is ~2 Å lower than the surrounding areas of phase I. Complete surface coverage by phase II is reached between 40 and 50% humidity.

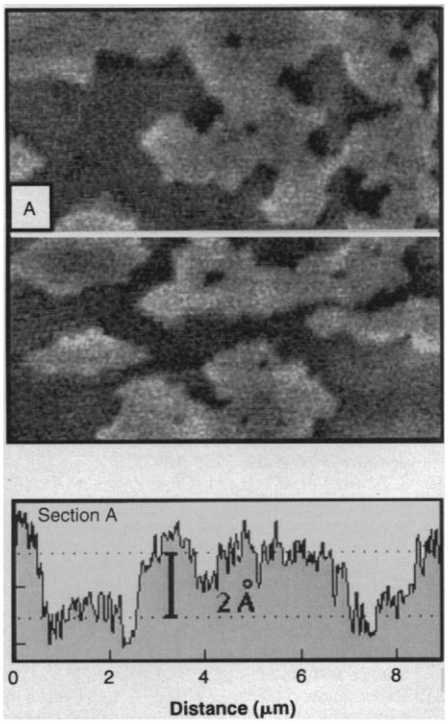

Fig. 3. Line profile across domains of phase I (dark) and phase II (bright) illustrating their apparent heights. The height of the domains of phase II is about 2 Å lower than the surrounding domains of phase I, indicating that the dielectric constant is lower in the regions covered by phase II than in phase I. Notice also the tendency of the domains edges to be straight lines with 60° and 120° angles.

domains of a different phase nucleated (Fig. 2). These domains increased in size until they covered the surface uniformly at 40 to 50% humidity. There are several interesting features of this second phase (which we call phase II). First is a reversal of contrast: The domains of phase II appear to be ~2 Å "lower" than the surrounding area of phase I water (Fig. 3). The height difference corresponds to a reduction in the attractive force over phase II areas of several tens of piconewtons, which is small compared with the total attractive force of ~10 nN. Second, the islands often have polygonal shapes, that is, the edges are often found to follow approximately straight lines forming angles of 60° and 120° (Figs. 3 and 4). By bringing the tip into contact with the substrate, the water layer is disrupted, and lattice-resolved images of mica are obtained. These images allowed us to determine the epitaxial relation between the water film and the substrate. There is a clear orientational preference of the domain edges along the close-packed directions of the mica (Fig. 5). This observation suggests a crystalline structure for phase II water, perhaps that of an ice bilayer.

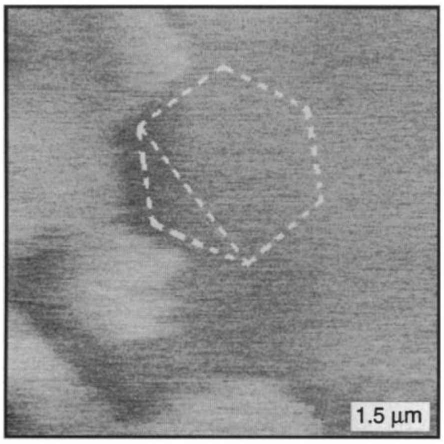

Fig. 4. Closeup of a boundary region between phase I and phase II domains showing the hexagonal symmetry. A hexagon has been drawn for visual reference. Image size is 1.5 µm by 1.5 µm. The edges of the hexagon are aligned with the mica crystallographic directions, as shown in Fig. 5.

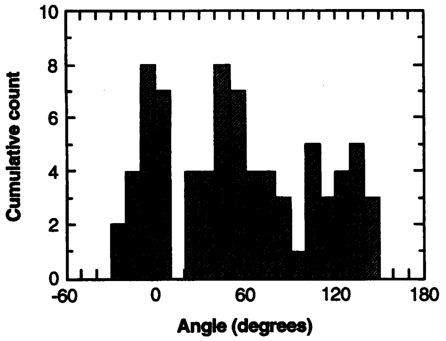

Fig. 5. Statistics of the orientation of island edges with respect to the crystallographic directions of the mica surface. The lattice of the latter is imaged by bringing the tip into contact with the substrate, a process that displaces the water.

When the humidity was decreased by the introduction of a desiccant material, the drying process could also be imaged. In Fig. 6, we show the evolution of the film structure as it evaporated while the humidity decreased from 37 to 21%. During the drying process, holes formed in the phase II domains. The dynamic nature of the adsorption-desorption process was revealed by the simultaneous formation of areas of phase II in regions occupied by phase I (while the humidity was above ~25%) in competition with the formation of holes in the phase II domains. As drying continued, all domains of phase II disappeared and no further contrast changes were observed (down to 18%).

The apparent height of the islands in both phase I and II (~2 Å) suggests that the thickness of the water layer is of molecular dimensions. This is supported by the ellipsometric measurements by Beaglehole and Christenson (*12*) that indicate that for humidities up to ~50%, the average thickness of the water film on mica is around 2 Å, that is, one molecular layer (or bilayer) thick. Muscovite mica is composed of layers of K^+ ions between aluminum silicate sheets. Mica cleaves along the ion planes to leave K^+ ions on each surface. We propose that phase I includes water molecules solvating K^+ ions. This interpretation is supported by infrared spectroscopy studies of layered silicates (clays) that show that when the water content is low, the molecules are tied into solvation shells around the intercalated ions. At higher water contents, the formation of nonsolvated water (hydrogen bonded) is observed. Similar results have been obtained for water adsorption on Pt(111) with coadsorbed K (*13*). We propose that once phase I is completed, the amount of hydrogen-bonded water increases, leading to ordered structures (phase II) with angular epitaxial relation with the mica lattice. The lower apparent height of phase II relative to phase I indicates that the dielectric constant is smaller in the former. We know from frequency-dependence studies (*11*) that the main contribution to the measured polarization force is from surface ion mobility. The smaller mobility of these ions in phase II relative to phase I would explain the observed contrast reversal. A reduced ionic mobility is also consistent with a solid (ice) structure of phase II.

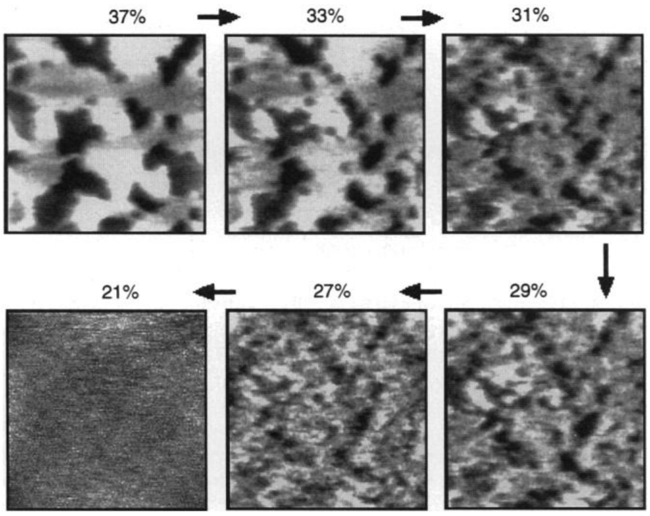

Fig. 6. The evaporation of a water film (phase II) on mica in a series of 2.3 µm by 2.3 µm images. The humidity decreases with time from the initial 37% value, after the water source (beaker with distilled water) is removed from the chamber and is replaced by a desiccant material. Drying proceeds by the formation of holes in the domains of phase II in competition with adsorption of water in phase I areas.

REFERENCES AND NOTES

1. Q. Du, E. Freysz, Y. R. Shen, *Phys. Rev. Lett.* **72**, 238 (1994).
2. J. D. Porter and A. S. Zinn, *J. Phys. Chem.* **97**, 1190 (1993).
3. See, for example, J. N. Israelachvili, *Chem. Scr.* **25**, 7 (1985); *Acc. Chem. Res.* **20**, 415 (1987).
4. J. Glosli and M. Philpott, *Proceedings of the Symposium on Microscopic Models of Electrolyte Interfaces* (Electrochemical Society, Pennington, NJ, 1993), vol. 93-5, p. 90.
5. C. Nöbl, C. Benndorf, T. E. Madey, *Surf. Sci.* **157**, 29 (1985); *ibid.* **194**, 63 (1988).
6. C. Y. Lee, J. A. McCammon, R. J. Rossky, *J. Chem. Phys.* **80**, 4448 (1984).
7. G. N. Patey and G. M. Torrie, *Chem. Scr.* **29A**, 39 (1989).
8. E. Spohr, *J. Phys. Chem.* 93, 6171 (1989).
9. K. Raghavan, K. Foster, M. Berkowitz, *Chem. Phys. Lett.* **177**, 426 (1991).
10. Y. Martin, D. W. Abraham, H. K. Wickramasinghe, *Appl. Phys. Lett.* **52**, 1103 (1988).
11. J. Hu, X.-D. Xiao, M. Salmeron, unpublished results.
12. D. Beaglehole and H. K. Christenson, *J. Phys. Chem.* **96**, 3395 (1992).
13. N. Kizhakevariam, I. Villegas, M. J. Weaver, unpublished results.
14. This work was supported by the Lawrence Berkeley Laboratory through the Director, Office of Energy Research, Basic Energy Science, Materials Science Division of the U.S. Department of Energy under contract DE-AC03-76SF00098. J.H. acknowledges a grant from the Academia Sinica and the Committee of Science and Technology of Shanghai (China).

13 October 1994; accepted 10 January 1995